Electronic structure and charge carriers in metallic DNA investigated by soft x-ray spectroscopy

J. B. MacNaughton,[1] E. Z. Kurmaev,[2] L. D. Finkelstein,[2] J. S. Lee,[3] S. D. Wettig,[4] and A. Moewes[1]
[1]*Department of Physics and Engineering Physics, University of Saskatchewan, 116 Science Place, Saskatoon, Saskatchewan S7N 5E2, Canada*
[2]*Institute of Metal Physics, Russian Academy of Sciences Ural Division, 620219 Yekaterinburg GSP-170, Russia*
[3]*Department of Biochemistry, University of Saskatchewan, 107 Wiggins Road, Saskatoon, Saskatchewan S7N 5E5, Canada*
[4]*College of Pharmacy and Nutrition, University of Saskatchewan, 110 Science Place, Saskatoon, Saskatchewan S7N 5C9, Canada*
(Received 6 February 2006; revised manuscript received 7 April 2006; published 22 May 2006)

Resonant inelastic x-ray scattering (RIXS) measurements of dried metallic DNA with metal ions incorporated inside the helix [(X)·M-DNA, X=Co,Ni], dried DNA with metal ions attached to the outside of the helix [(X)·B-DNA, X=Co,Ni], and dried double-strand DNA (B-DNA) are presented. The metal *L* edge RIXS spectra show that the $I(L_2)/I(L_3)$ intensity ratio can be used as a probe of metallicity in 3*d* metal-containing systems because of the influence of nonradiative Coster-Kronig transitions. Using this technique it is found that (X)·B-DNA has fewer mobile charge carriers than (X)·M-DNA. X-ray absorption measurements at the *L* edge of the 3*d* metals are compared to density functional calculations to confirm that spectral features are not simply results of residual metal impurities. Nitrogen RIXS measurements reveal that the occupied electronic states are more localized in B-DNA than in (X)·M-DNA systems.

DOI: 10.1103/PhysRevB.73.205114 PACS number(s): 71.20.Rv, 78.70.En, 78.70.Dm, 71.15.Mb

I. INTRODUCTION

Charge transfer in DNA was first suggested in 1962 by Eley and Spevey,[1] nearly ten years after the discovery of the DNA double helix structure.[2] Electron transport through DNA molecules has received great attention in recent years because of possible applications ranging from nanoelectronic devices[3,4] to long-range detection of damage in DNA.[5,6] However, the results of experiments investigating the conductivity of DNA are often found to be contradictory, with electrical properties ranging from insulating,[7–10] semiconducting,[4,11,12] highly conductive,[3] to superconducting[13] behavior.

Differences in the type and setup of the measurement, the sample preparation techniques and the environmental conditions all contribute to the variety of experimental conductivity results found in the literature. Specifically, the interaction of the DNA molecules with the substrate and the interaction at the contact points between the DNA and electrodes are primary factors, which are difficult to control with a microscopic setup required to measure conductivity directly.[14] As a result, the development of indirect methods (free of contacts) for probing carriers in DNA systems is of great interest.

In general, it is supposed that DNA is a wide band gap semiconductor.[12] Significant research has been done to employ metal ions to increase the conductivity of DNA, as described in a recent review article.[15] For example, the conductivity of DNA can be improved by the deposition of silver atoms along the helical structure, but this process is essentially irreversible.[7] Another possibility is to convert dried double-strand DNA (B-DNA) to dried metallic DNA with metal ions incorporated inside the helix [(X)·M-DNA] by the addition of divalent metal ions (Zn^{2+}, Co^{2+}, and Ni^{2+}) at *p*H values above 8.5.[16]

The electron transport through (Zn)·M-DNA molecules has been monitored mainly by fluorescence spectroscopy of duplexes labeled at opposite ends with donor and acceptor fluorophores.[16] Direct measurements of conductivity have confirmed that (Zn)·M-DNA exhibits metallic-like conductivity and electron transfer can be observed in duplexes as long as 15 μm.[12]

Investigating the electronic structure with soft x-ray absorption (XAS) and emission (XES) spectroscopy using synchrotron radiation presents a spectroscopic approach that provides valuable information about the occupied and unoccupied partial densities of states without the requirement of a microscopic setup. Previous experiments involving (X)·M-DNA have measured the current versus voltage (*I-V*) relationship using a microscopic setup, while this current study incorporates a spectroscopic and macroscopic approach. Our main focus for this study is to use spectroscopy to probe the interaction of the metal ions with the DNA molecules and determine what influence the metal has on the electronic structure of DNA.

Recently, we have shown that resonant inelastic x-ray scattering (RIXS) measurements near the *L* absorption edge of a 3*d* metal can be used for probing carriers in Co-doped TiO_2 and other diluted magnetic semiconductors.[17] The *L* edge spectra of 3*d* elements are sensitive to the metallicity of the system. We have used RIXS measurements to study carriers in the (X)·M-DNA and (X)·B-DNA (X=Co,Ni) systems. Cobalt and nickel *L* edge x-ray absorption measurements are compared to density functional calculations of several model compounds to determine the origin of spectral contributions. Nitrogen *K* edge RIXS measurements are presented to compare the degree of localization of the electronic nitrogen states in B-DNA and (X)·M-DNA.

II. SAMPLE PREPARATION

In general, (X)·M-DNA can be produced from all duplex sequences at *p*H values between 8 and 9 with Zn^{2+}, Ni^{2+} and Co^{2+}, but not with Mg or Mn ions.[18] The conditions under

which (X)·M-DNA can form are fairly restricted. If the *p*H is too low (X)·M-DNA will not form and if the *p*H is too high, the metal salts will precipitate. (X)·M-DNA can be readily converted to B-DNA upon lowering the *p*H value, which suggests that the double helical structure remains intact.[18] If metal ions are added to a B-DNA solution and the *p*H is not sufficiently high to form (X)·M-DNA, the result will be a B-DNA complex with metal ions attached only to the outside of the helix, rather than directly inside the nucleobases.[16] This structure is referred to as (X)·B-DNA for this study. It is likely that both the (X)·B-DNA and (X)·M-DNA powdered samples will have excess metal ions which are not bonded directly to the DNA strand.

All samples of DNA were prepared in a buffer solution (required to stabilize the *p*H), then dried using lyophilization, and measured in powder form. Calf thymus DNA (42% G-C, 58% A-T) and tris(hydroxymethyl)aminomethane (TRIS) buffer were purchased from Sigma. Metal chloride salts were obtained from Aldrich. A concentrated DNA stock solution (~1.5 mg/ml) was prepared and diluted to a final concentration of 100 μg/ml. The DNA was sheared by five passages of the stock solution through a syringe needle.[19] The B-DNA sample was prepared by lyophilization of 25 ml of 100 μg/ml calf thymus DNA prepared in 10 mM TRIS buffer (*p*H 7.5). (X)·B-DNA samples were prepared by the addition of $NiCl_2$ or $CoCl_2$ (0.1 mM) to the *p*H 7.5 B-DNA. The (X)·M-DNA samples were prepared using TRIS buffer (*p*H adjusted with HCl) and 0.1 mM $NiCl_2$ or $CoCl_2$ at *p*H 8.5 according to the technique previously described.[16,18]

III. EXPERIMENT

Beamline 8.0.1 at the Advanced Light Source, located at Lawrence Berkeley National Laboratory, was used for the soft x-ray spectroscopic measurements included in this study. The x-ray absorption spectra (XAS) presented in this study were measured in total electron yield mode. The resolution for the 3*d* metal absorption spectra is about 0.2 eV at the nickel and cobalt edges. The emitted radiation is partially collected in a Rowland circle-type spectrometer with spherical gratings and recorded with an area-sensitive multichannel detector for the emission measurements. The details of this end station are described elsewhere.[20] The experimental resolution for the nickel $L_{2,3}$ x-ray emission spectra is 2.2 eV full width at half maximum (FWHM), resolution for the cobalt $L_{2,3}$ x-ray emission spectra is 1.8 eV FWHM, and the resolution for the nitrogen $K\alpha$ x-ray emission region is 0.75 eV FWHM. All absorption and emission spectra are normalized to the number of photons incident on the sample, monitored by a highly transparent gold mesh located in front of the sample chamber. The angle of incident radiation was 60° and the same experimental geometry was used for all measurements. The energy scales of the 3*d* metal absorption spectra were calibrated using reference spectra for the nickel[21] and cobalt edges.[22] To allow for peak ratio comparisons, cobalt and nickel *L* edge RIXS spectra were shifted to align with energy values presented by Bearden.[23] Energy calibration for the nitrogen edge RIXS was completed using measurements of a reference sample (*h*-BN) and shifting the energy using known energy values.[24]

For comparison purposes results from previous studies of CoO are included to compare with our measurements of cobalt metal, nickel metal, NiO, and the DNA samples. Included in this study is resonant x-ray emission for CoO measured by Magnuson *et al.*[22] Nonresonant x-ray emission data of CoO measured with a lab source is also presented for comparison.

IV. CALCULATIONS

The program STOBE[25] was designed to analyze the electronic structure of molecules and is used to simulate x-ray absorption spectra. The program uses a linear combination of Gaussian-type orbitals approach to form self-consistent solutions of the Kohn-Sham density functional theory (DFT) equations. Triple-zeta plus valence polarization (TZVP) Huzinaga orbital basis sets and A5 auxiliary basis sets derived from the TZVP basis sets were used in this study.[26]

The calculations of the absorption spectra with STOBE use a combination of the transition potential method and a double basis set technique integrated into density functional theory. In this approach, the core electron undergoing the excitation is replaced by a half-occupied core hole.[27] The excited state orbitals are then calculated, and the probabilities for transitions between the core level and the unoccupied states are determined. To assist with convergence in the 3*d* metal XAS calculations, the half core hole was spread evenly across the three $2p_{3/2}$ core orbitals.

Several compounds were selected to represent a sampling of possible residual metal structures that could form from the metal ions not directly bonded to the DNA molecules. Metal chlorides were included since $CoCl_2$ and $NiCl_2$ were added to the solution to provide metal ions during sample preparation. The metal oxides CoO, CoOH, NiO, and NiOH represent other possible structures that may form through various interactions with the buffer solution. These selections are not intended to represent all of the possible structures that will exist in the sample, just some of the common ones. Models of the NiO, $(NiOH)^+$, $NiCl_2$, $(CoO)^+$, CoOH and $(CoCl_2)^+$ molecules were first created using SPARTAN 04 (Ref. 28) and then optimized using STOBE.

The complexity of DNA results in challenges when developing analytical and theoretical approaches to understanding the biomolecules. This often results in applying models of simpler systems to the more complicated picture. To help determine spectral contributions from the metal ions interacting directly with the B-DNA molecule, it was desirable to create a model of the nucleobases of (X)·M-DNA. The helical structure of DNA and the nucleobase pairs are displayed in Fig. 1, along with the numbering scheme of the atoms in the nucleobases. One of the proposed structures of (X)·M-DNA shows a metal ion replacing the hydrogen atom at the N3 position of thymine and the N1 position of guanine of every base pair, which is supported by nuclear magnetic resonance measurements,[18] but not yet confirmed by crystallographic data. Previous studies involving the interaction of DNA base pairs with Group IIa and Group IIb metal cations have presented models with the cations interacting with the N7 of adenine and the N7 and O6 atoms of guanine.[29–31] In

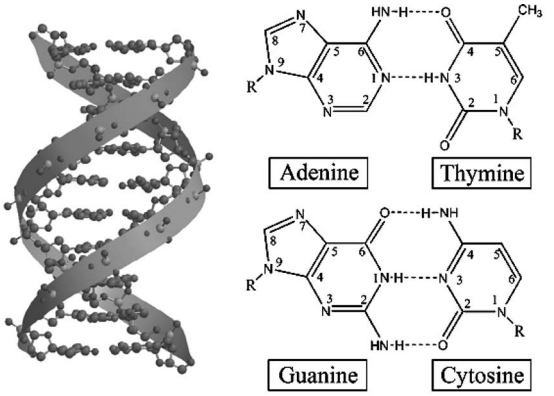

FIG. 1. Structure of a DNA molecule is shown on the left (ten nucleobase pairs). The ribbons follow the phosphate backbone demonstrating the helical shape and the stack of nucleobase pairs occurs in the center of the helix. Complementary Watson-Crick adenine-thymine and guanine-cytosine nucleobase pairs are shown in detail on the right, and the diagrams include the atom numbering scheme.

general, the N7 sites of guanine and adenine are preferable metal binding sites,[32,33] however a modified adenine-thymine base pair with the proton at the N3 location of thymine replaced with a Pt(II) ion has been found for the mixed 1-methylthymine, 9-methyladenine complex of *trans*-$[Pt(II)(NH_2Me)_2]$.[32] Metal ion interactions with the N3 site are possible but less prevalent than bonding with the N7 site, however if an increase in pH effectively deprotonates the N3 site, it may increase the likelihood of a metal ion binding at that site.[33]

Previously, DFT calculations of a Zn(II) guanine-cytosine M-DNA nucleobase pair were attempted, but it was found to be difficult to find a planar equilibrium structure.[34] This may indicate problems with the model, or that the inclusion of stacking interactions is important when optimizing the structure. For our study we desired to calculate the effects of the metal-nucleobase interaction on x-ray absorption spectra and have chosen to use the originally proposed model for simplicity. The hydrogen atom at the N3 position of thymine and the N1 position of guanine were replaced with a metal ion (Ni) or metal atom (Co) and the Watson-Crick nucleobases were allowed to rotate by 20° around an axis perpendicular to the plane of the bases, in order to allow the bond length between the metal and the nitrogen to increase to 2 Å.[16] XAS spectra were calculated for the nickel adenine-thymine (Ni-AT), nickel guanine-cytosine (Ni-GC) nucleobase pairs and the equivalent structures with cobalt (Co-AT and Co-GC) using STOBE.

Gaussian linewidths used for the simulated spectra were 1.0 eV (FWHM) up to the ionization potential and then linearly increasing to 4.0 eV (FWHM) over the next 10 eV. These linewidths were chosen to correspond to the experimentally observed results. In all cases the theoretical spectra have been shifted in energy to align with the experimental data. The minimum intensity value has been set to zero for all spectra.

V. RESULTS AND DISCUSSION

Figures 2 and 3 show the cobalt and nickel $2p$ x-ray absorption spectra, respectively. Transition metal $2p$ edge absorption spectroscopy has been an effective technique for examining the electronic structure of biological systems, in particular determining the oxidation states and spin states of Ni containing enzymes.[35,36] The metal $2p$ spin orbit interaction splits the spectrum into two sections, which consist of the $2p_{3/2}$ (L_3) and the $2p_{1/2}$ (L_2) features. The multiplet structure in the spectra is the result of the Coulomb and exchange interactions between the $3d$ shell and the core hole and this fine structure can reveal information about the transition metal oxidation state. Specifically for the Ni(II) state, unique spectral features can distinguish between the $3d^8$ high and low spin configurations.[37] It is found that Ni(I) spectra exhibit no multiplet structure due to a full d shell in the final state, high spin Ni(II) spectra have multiplet structure on the high energy slope of the L_3 peak and a broad or split L_2 edge, low spin Ni(II) spectra have minimal multiplet features on the L_3 peak and a sharper L_2 edge, ionic Ni(III) multiplet features are found on the low energy side of the L_3 peak and covalently bonded Ni(III) has broad features lacking multiplet structure.[35] The experimental spectra in Fig. 3 show multiplet structure on the high energy side of the L_3 peak, indicating a high spin Ni(II) configuration for the nickel samples. Octahedral, tetrahedral, or square planar symmetry may result from this configuration. Similarly, using the XAS spectra as fingerprints of the metal coordination for the cobalt edge in Fig. 2 and comparing to multiplet calculations and spectra of reference compounds, it is found that the cobalt coordination in our metallic DNA samples is most likely Co(II) with tetrahedral-type symmetry.[38,39]

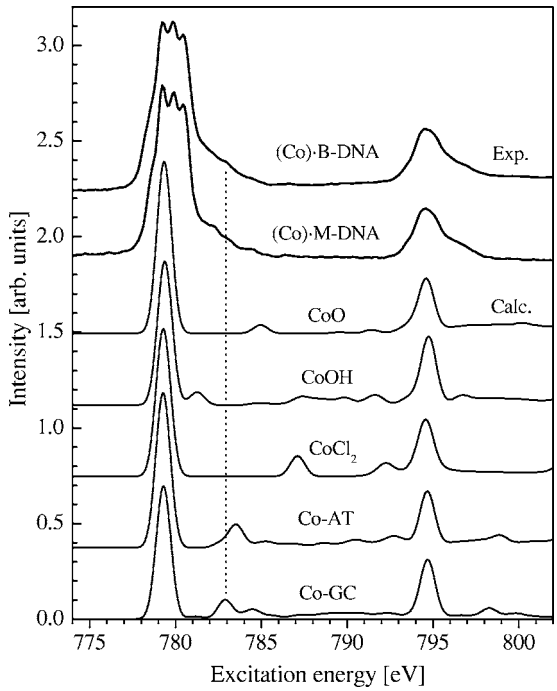

FIG. 2. Experimental cobalt $2p$ XAS spectra of (Co)·B-DNA and (Co)·M-DNA compared to theoretical spectra of CoO, CoOH, $CoCl_2$, Co-AT, and Co-GC. The vertical dotted line has been added to assist with comparing spectral features and an offset to the y axis has been added for clarity.

Although our techniques probe all metal ions in the sample, it is important for this study that the spectra are not

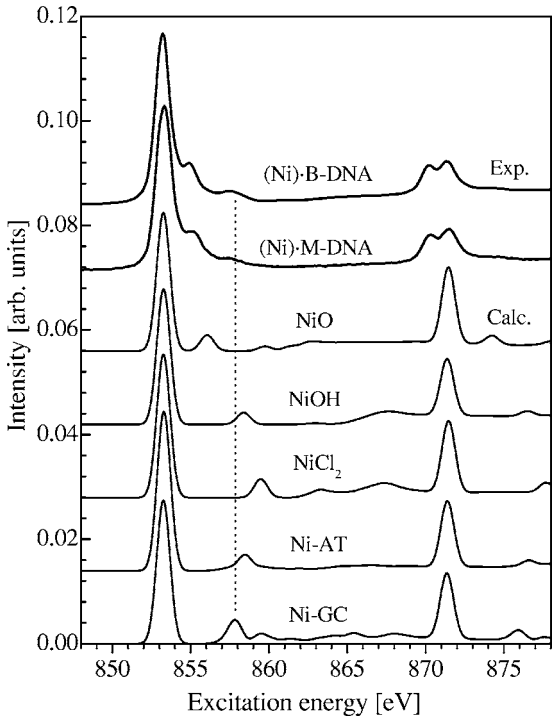

FIG. 3. Experimental nickel $2p$ XAS spectra of (Ni)·B-DNA and (Ni)·M-DNA compared with theoretical spectra of NiO, NiOH, $NiCl_2$, Ni-AT, and Ni-GC. A vertical dotted line has been added to assist with comparing spectral features and an offset to the y axis has been added for clarity.

dominated by contributions from residual metal structures. By comparing the spectra of (X)·B-DNA and (X)·M-DNA with simulations of various model compounds intended to represent excess metal structures (CoO, CoOH, $CoCl_2$, NiO, NiOH, and $NiCl_2$), it is found that the spectra of the model compounds do not seem to be very similar to the spectra of the DNA samples. By comparing the theoretical spectra of the compounds CoO, $CoCl_2$, and $NiCl_2$ to the experimental spectra, it is seen that these structures have minimal impact on the experimental results. The calculations of CoOH, NiO, and NiOH display features that are seen in the measurements of the DNA, including the first shoulder after the main L_3 peak, usually associated with oxidation. However, the calculations do not characterize all of the experimental features. This indicates that the spectra are not dominated by residual metal structures; rather they include influence from both the metal-DNA interaction and the excess metal.

The calculations of the cobalt and nickel M-DNA nucleobase pairs have been included to model the interaction of the metal ion with the DNA strand. The XAS spectra for both the (X)·B-DNA and (X)·M-DNA samples are very similar, and both have features that seem to correspond to the calculations used to model the metal-DNA interaction. These features are indicated in Figs. 2 and 3 by the dotted lines. While the XAS results do not prove that the models are the correct structures for the metallic nucleobase pairs, they do reveal that the spectra are influenced by the metal ions interacting with the DNA strands.

The $L\beta_1$ and $L\alpha_{1,2}$ x-ray emission from $3d$ elements corresponds to x-ray transitions from the occupied $3d4s$ valence states to the $2p_{1/2}$ and $2p_{3/2}$ core levels when neglecting higher multipole transitions, correlation effects, and the influence of the core hole relaxation. For free atoms with a fully occupied d shell, the integral intensity ratio of the L_2 and L_3 XES lines, $I(L_2)/I(L_3)$, is determined by the statistical population of the $2p_{1/2}$ and $2p_{3/2}$ levels. Therefore, the intensity ratio should be equal to $\frac{1}{2}$ when not taking into account nonradiative transitions. Condensing the free $3d$ atoms to a solid state can cause this ratio to change from the predicted value of $\frac{1}{2}$ due to the electrostatic interaction between $2p$ core holes and electrons in the unfilled $3d$ shell. This allows the integral intensity ratio $I(L_2)/I(L_3)$ to provide information concerning the $2p$-$3d$ interaction.

Aside from the $2p$-$3d$ electrostatic interaction, nonradiative $L_2L_3M_{4,5}$ Coster-Kronig (CK) transitions can also influence the intensity ratio $I(L_2)/I(L_3)$ in $3d$ metal solids. Generally, CK transitions partially depopulate the L_3 state when radiationless transitions from the L_3 to the L_2 level occur before the emission process can take place. The transition energy can be released via emission of $3d$ Auger electrons. The probability for this process to occur in free atoms is minimal, but it is strongly enhanced in condensed matter systems. This enhancement is due to the screening of intraatomic electron interactions in solids and it leads to a decrease in the energy difference between initial and final states of the nonradiative CK process. This effect is particularly prominent in metals.[40,41] In metals, the optical potential reaches its maximum value at plasma vibrations of about 10–15 eV, which coincides with the magnitude of the $L_{2,3}$ level spin-orbit splitting, at which point it will only depend on the concentration of the conducting electrons.[42] When an L_3 electron relaxes to the L_2 level the relaxation energy is transferred to the electron cloud, giving rise to plasma vibrations.

Taking into account these factors, we used the following expression for the $I(L_2)/I(L_3)$ ratio:[43]

$$\frac{I(L_2)}{I(L_3)} = \frac{1 - f_{2,3}}{f_{2,3} + \mu_3/\mu_2}, \tag{1}$$

where $f_{2,3}$ is the probability for the CK process to occur and μ_3/μ_2 is the ratio of the absorption coefficients for the excitation energies at the L_3 and the L_2 threshold. When the excitation energy is set well above the L_2 threshold (nonresonant regime), μ_3/μ_2 has a constant value of 2 for all elements. Therefore, the ratio $I(L_2)/I(L_3)$ is determined only by the parameter $f_{2,3}$, which increases for a given element (Co and Ni in our case) with the number of mobile d carriers available.[41] For the resonant excitation, the parameter μ_3/μ_2 changes with the excitation energy and becomes minimal when exciting at the L_2 threshold.[43] This results in a strongly increased excitation at the L_2 threshold.

The influence of nonradiative CK transitions for the nonresonant $L\alpha,\beta$ NXES excited well above the L_2 edge and the resonant $L\alpha,\beta$ RXES excited at the L_2 edge can be seen in Figs. 4 and 5. For both resonant and nonresonant spectra the $I(L_2)/I(L_3)$ intensity ratio for (X)·M-DNA and (X)·B-DNA differs and the spectra occupy the intermediate positions between the metal oxide and the pure metal spectra. It is typical

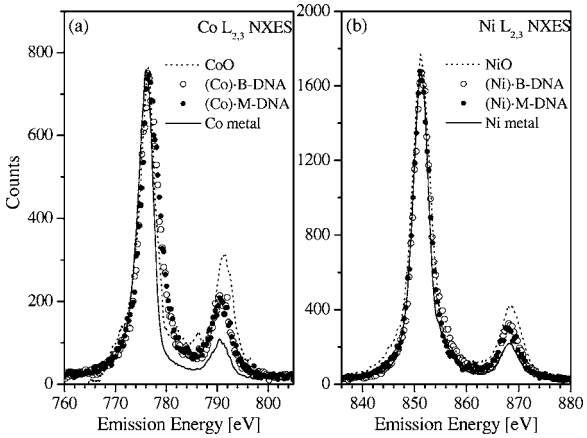

FIG. 4. $L\alpha,\beta$ NXES spectra of (X)·B-DNA and (X)·M-DNA.

that the $I(L_2)/I(L_3)$ intensity ratio increases upon going from pure $3d$ metals to their oxides, because the nonradiative $L_2L_3M_{4,5}$ CK transition probability is expected to be lower for $3d$ metal oxides than for metals due to the reduced number of electrons.

The intermediate position of the $I(L_2)/I(L_3)$ intensity ratio of (X)·M-DNA between the metal oxide and the pure metal indicates that the number of carriers in (X)·M-DNA systems is higher than in the insulating metal oxide and less than in the case of the pure metal. The higher sensitivity of resonant spectra with respect to nonresonant spectra allowed differences in the $I(L_2)/I(L_3)$ intensity ratio between (X)·B-DNA and (X)·M-DNA to be found in Fig. 5. For both the cobalt and nickel systems, we conclude that the number of carriers is higher for (X)·M-DNA than for (X)·B-DNA systems, but is still less than in the case of a pure metal. Previous results have shown that B-DNA is less conducting than (X)·M-DNA (Ref. 44) and our results are in agreement.

We have also used nitrogen RIXS spectra to investigate the electronic structure of the DNA samples. In the DNA structure the nitrogen atoms are located exclusively in nucleobases, not in the backbone, allowing the electronic orbital features of the nucleobases to be probed directly. Figure 6 shows the RIXS spectra of B-DNA, (Co)·M-DNA and

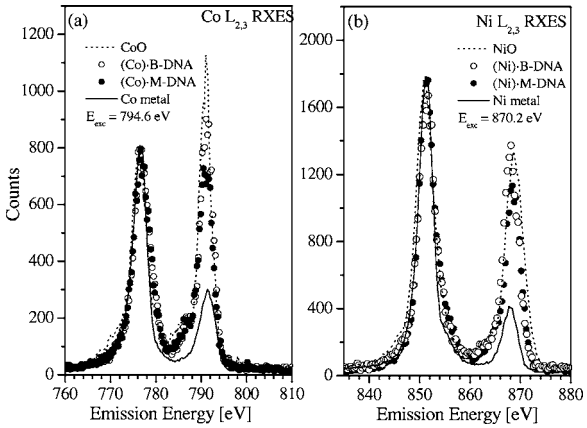

FIG. 5. $L\alpha,\beta$ RXES spectra of (X)·B-DNA and (X)·M-DNA.

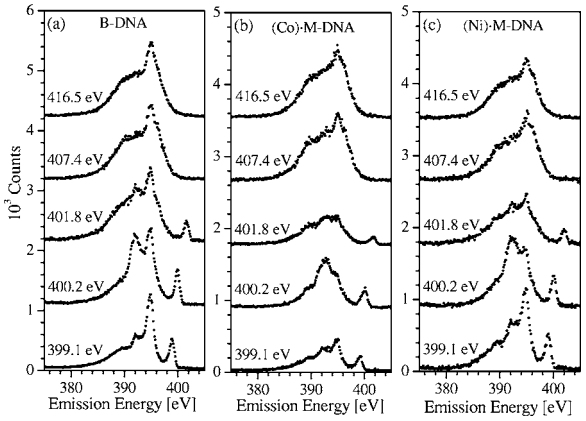

FIG. 6. Nitrogen RIXS spectra of (a) B-DNA, (b) (Co)·M-DNA, and (b) (Ni)·M-DNA. The excitation energy is labeled on the left side of each spectrum. An offset to the y axis has been added for clarity.

(Ni)·M-DNA excited near the N $1s$ threshold. Since the TRIS buffer contains nitrogen atoms, it is important to note that the nitrogen in DNA and in the buffer both influence this spectrum, and it is not possible to distinguish between the two contributions. However, all three samples were prepared with the same TRIS buffer, ensuring that the measurements are comparable.

Figure 6 shows that unique results are found in the nitrogen RIXS data for each of the DNA samples. The RIXS technique is a direct probe of the occupied electronic states of the systems. The nitrogen emission results from a multitude of transitions occurring from occupied states with p symmetry to the open K shells in the various nitrogen atoms. Since emission features in the RIXS spectra do not track the excitation energy it is assumed that features are not the result of inelastic loss features, rather they are the consequence of normal emission processes. The intensity changes of the emission peaks in the spectra measured at the various excitation energies are caused by transitions to different intermediate states. The sharp high-energy features in the resonant spectra are elastic peaks.

Differences observed in nitrogen spectra are further proof that we are probing structural differences in the DNA samples with the metal RIXS spectra, not just excess transition metal ions. Comparing the B-DNA data to the (X)·M-DNA spectra it is found that B-DNA has sharper features at all excitation energies. This is especially true for the resonant energies, where features are much less defined for the (X)·M-DNA systems. At an incoming energy of 400.2 eV, the B-DNA spectrum has a well-defined two peak structure centered at 393.4 eV, while in the metallic DNA samples for the same excitation energy the peak splitting is not as pronounced. The broadening of these peaks in the RIXS spectra of (Co)·M-DNA and (Ni)·M-DNA directly indicates that the valence states are more delocalized for the (X)·M-DNA systems than in the B-DNA sample.

VI. CONCLUSION

In this study we characterize the electronic structure of the (X)·M-DNA and (X)·B-DNA systems using RIXS spectra

near the transition metal L and nitrogen K edges. The $I(L_2)/I(L_3)$ intensity ratios in the metal L edge spectra are found to be reduced for the (X)·M-DNA compared to the (X)·B-DNA system, which is attributed to a higher number of charge carriers in the first system. By using the XAS spectra as fingerprints of the metal coordination, it is found that the cobalt coordination in our metallic DNA samples is most likely Co(II) in a tetrahedral-type symmetry, and a high spin Ni(II) coordination was determined for the nickel compounds. It is found that metal $2p$ XAS spectra are influenced by the interaction of the metal ions with the DNA molecules. While this agreement does not prove that the models are correct for the (X)·M-DNA structure, it does show that we are indeed probing the interaction of metal ions with the DNA samples, not simply excessive metal impurities found in the local chemical environment. Further evidence that we are investigating the metal-DNA interaction with our technique is seen in the differences found in the nitrogen spectra. The well-defined, sharp peaks of the nitrogen RIXS spectra indicate localized occupied electronic states in B-DNA. The broadening of these features directly suggests delocalization of the occupied electronic states in the (X)·M-DNA systems. Further understanding of the conductive mechanisms in DNA systems is a necessary precursor to the ability to manipulate biomolecules for applications in fields such as nanoelectronics.

ACKNOWLEDGMENTS

Funding by the Natural Sciences and Engineering Research Council of Canada (NSERC), the Canada Research Chair Program, the Research Council of President of the Russian Federation (Grant No. NSH-4192.2006.2), and the Russian Science Foundation for Basic Research (Project No. 05-02-16438) is gratefully acknowledged. The work at the Advanced Light Source at Lawrence Berkeley National Laboratory was supported by U.S. Department of Energy (Contract No. DE-AC03-76SF00098).

[1] D. D. Eley and D. I. Spivey, Trans. Faraday Soc. **58**, 411 (1962).
[2] J. D. Watson and F. H. C. Crick, Nature (London) **171**, 737 (1953).
[3] H. W. Fink and C. Schönenberger, Nature (London) **398**, 407 (1999).
[4] D. Porath, A. Bezryadin, S. de Vries, and C. Dekker, Nature (London) **403**, 635 (2000).
[5] S. O. Kelley and J. K. Barton, Science **283**, 375 (1999).
[6] R. G. Endres, D. L. Cox, and R. R. P. Singh, Rev. Mod. Phys. **76**, 195 (2004).
[7] E. Braun, Y. Eichen, U. Sivan, and G. Ben-Yoseph, Nature (London) **391**, 775 (1998).
[8] P. J. de Pablo, F. Moreno-Herrero, J. Colchero, J. G. Herrero, P. Herrero, A. M. Baro, P. Ordejon, J. M. Soler, and E. Artacho, Phys. Rev. Lett. **85**, 4992 (2000).
[9] A. J. Storm, J. van Noort, S. de Vries, and C. Dekker, Appl. Phys. Lett. **79**, 3881 (2001).
[10] P. Tran, B. Alavi, and G. Gruner, Phys. Rev. Lett. **85**, 1564 (2000).
[11] K. H. Yoo, D. H. Ha, J. O. Lee, J. W. Park, J. Kim, J. J. Kim, H. Y. Lee, T. Kawai, and H. Y. Choi, Phys. Rev. Lett. **87**, 198102 (2001).
[12] A. Rakitin, P. Aich, C. Papadopoulos, Y. Kobzar, A. S. Vedeneev, J. S. Lee, and J. M. Xu, Phys. Rev. Lett. **86**, 3670 (2001).
[13] A. Y. Kasumov, M. Kociak, S. Gueron, B. Reulet, V. T. Volkov, D. V. Klinov, and H. Bouchiat, Science **291**, 280 (2001).
[14] H. Cohen, C. Nogues, R. Naaman, and D. Porath, Proc. Natl. Acad. Sci. U.S.A. **102**, 11589 (2005).
[15] J. Richter, Physica E (Amsterdam) **16**, 157 (2003).
[16] P. Aich, S. L. Labiuk, L. W. Tari, L. J. T. Delbaere, W. J. Roesler, K. J. Falk, R. P. Steer, and J. S. Lee, J. Mol. Biol. **294**, 477 (1999).
[17] G. S. Chang, E. Z. Kurmaev, D. W. Boukhvalov, L. D. Finkelstein, D. H. Kim, T.-W. Noh, A. Moewes, and T. A. Callcott, J. Phys.: Condens. Matter (submitted).
[18] J. S. Lee, L. J. P. Latimer, and R. S. Reid, Biochem. Cell Biol. **71**, 162 (1993).
[19] R. E. Pyeritz, C. A. Thomas, and R. A. Schlegel, Biochim. Biophys. Acta **272**, 504 (1972).
[20] J. J. Jia, T. A. Callcott, J. Yurkas, A. W. Ellis, F. J. Himpsel, M. G. Samant, J. Stöhr, D. L. Ederer, J. A. Carlisle, E. A. Hudson, L. J. Terminello, D. K. Shuh, and R. C. C. Perera, Rev. Sci. Instrum. **66**, 1394 (1995).
[21] G. van der Laan, J. Zaanen, G. A. Sawatzky, R. Karnatak, and J. M. Esteva, Phys. Rev. B **33**, 4253 (1986).
[22] M. Magnuson, S. M. Butorin, J.-H. Guo, and J. Nordgren, Phys. Rev. B **65**, 205106 (2002).
[23] J. A. Bearden, Rev. Mod. Phys. **39**, 78 (1967).
[24] V. A. Fomichev and M. A. Rumsh, J. Phys. Chem. Solids **29**, 1015 (1968).
[25] K. Hermann, L. G. M. Pettersson, M. E. Casida, C. Daul, A. Goursot, A. Koester, E. Proynov, A. St-Amant, D. R. Salahub, V. Carravetta, H. Duarte, N. Godbout, J. Guan, C. Jamorski, M. Leboeuf, V. Malkin, O. Malkina, M. Nyberg, L. Pedocchi, F. Sim, L. Triguero, and A. Vela, STOBE—DEMON *version 2.1* (2005).
[26] K. Hermann and L. G. M. Pettersson, *Documentation for* STOBE*2005 (Version 2.1)* (Berlin, 2005).
[27] L. Triguero, L. G. M. Pettersson, and H. Agren, Phys. Rev. B **58**, 8097 (1998).
[28] Wavefunction, Inc., SPARTAN 04, Irvine (2004).
[29] J. V. Burda, J. Sponer, J. Leszczynski, and P. Hobza, J. Phys. Chem. B **101**, 9670 (1997).
[30] J.Šponer, J. V. Burda, M. Sabat, J. Leszczynski, and P. Hobza, J. Phys. Chem. A **102**, 5951 (1998).
[31] N. Gresh and J. Šponer, J. Phys. Chem. B **103**, 11415 (1999).
[32] B. Lippert, J. Chem. Soc. Dalton Trans. **21**, 3971 (1997).
[33] H. Sigel, Chem. Soc. Rev. **22**, 255 (1993).
[34] R. Di Felice, A. Calzolari, and H. Zhang, Nanotechnology **15**, 1256 (2004).
[35] H. X. Wang, C. Y. Ralston, D. S. Patil, R. M. Jones, W. Gu, M. Verhagen, M. Adams, P. Ge, C. Riordan, C. A. Marganian, P.

Mascharak, J. Kovacs, C. G. Miller, T. J. Collins, S. Brooker, P. D. Croucher, K. Wang, E. I. Stiefel, and S. P. Cramer, J. Am. Chem. Soc. **122**, 10544 (2000).

[36] H. X. Wang, D. S. Patil, W. W. Gu, L. Jacquamet, S. Friedrich, T. Funk, and S. P. Cramer, J. Electron Spectrosc. Relat. Phenom. **114**, 855 (2001).

[37] G. van der Laan, B. T. Thole, G. A. Sawatzky, and M. Verdaguer, Phys. Rev. B **37**, 6587 (1988).

[38] L. Drozdová, R. Prins, J. Dědeček, Z. Sobalík, and B. Wichterlová, J. Phys. Chem. B **106**, 2240 (2002).

[39] D. Bazin, I. Kovács, L. Guczi, P. Parent, C. Laffon, F. De Groot, O. Ducreux, and J. Lynch, J. Catal. **189**, 456 (2000).

[40] M. O. Krause, J. Phys. Chem. Ref. Data **8**, 307 (1979).

[41] V. I. Grebennikov, Surf. Invest. X-Ray Synchrotron Neutron Tech. **11**, 41 (2002).

[42] V. I. Grebennikov, Phys. Met. Metallogr. **89**, 425 (2000).

[43] E. Z. Kurmaev, A. L. Ankudinov, J. J. Rehr, L. D. Finkelstein, P. F. Karimov, and A. Moewes, J. Electron Spectrosc. Relat. Phenom. **148**, 1 (2005).

[44] S. D. Wettig, C.-Z. Li, Y.-T. Long, H.-B. Kraatz, and J. S. Lee, Anal. Sci. **19**, 23 (2003).